PNAS RESEARCH ARTICLE | MEDICAL SCIENCES DEVELOPMENTAL BIOLOGY OPEN ACCESS

An atlas of early human mandibular endochondral and osteogenic paracrine signaling regions of Meckel's cartilage

Zongshan Shen[a,b,c,1], Ran Zhang[a,d,1], Xinyue Chen[a], Guan Yang[e], Yuanchun Si[a], Tianxing Yan[d], Suwen Chen[f], Bin Cheng[c], Xiaoshan Wu[a,g], Di Chen[h], Dong Zhang[a,b], Guozhi Xiao[i], Jian-Kang Zhu[j,2], and Songlin Wang[a,b,g,k,2]

Affiliations are included on p. 10.

Contributed by Jian-Kang Zhu; received October 6, 2024; accepted February 11, 2025; reviewed by Jeremy B. Green, Xianfeng Lin, and Noriaki Ono

The mandible, also known as the lower jaw, is the only bone in the skull that can move and is essential for speaking and chewing. Meckel's cartilage (MC) is a temporary structure that supports the formation of the mandible, but how MC is involved in the ossification of the mandible is poorly understood. Through the use of single-cell RNA sequencing and single-cell spatial transcriptomics analyses, a spatiotemporal atlas of MC in human fetuses from 7 to 15 wk postconception was established, highlighting the role of MC in the ossification of the mandible. Importantly, we revealed that two populations of MC contributed to mandibular ossification through different mechanisms. The anterior MC can differentiate into osteolineage cells, as shown in an in vivo lineage tracing mouse model. The intermediate MC facilitates intramembranous ossification through cell–cell communications, possibly through signaling ligands like *BMP5*, *BMP7*, *SEMA3A*, *PDGFC*, and *FGF7*. This study suggests that MC plays a crucial role in mediating mandibular ossification through distinct mechanisms, providing valuable insights for understanding oral and craniofacial diseases and disorders in the future.

human fetal mandible development | Meckel's cartilage | single-cell RNA sequencing | single-cell spatial transcriptomics | cell atlas

Significance

This research identified two distinct components of Meckel's cartilage (MC) that play different roles in the formation of the mandible in humans. Single-cell RNA sequencing and single-cell spatial transcriptomics revealed that the anterior MC is responsible for endochondral ossification, whereas the intermediate MC controls intramembranous ossification. These findings, supported by mouse studies, provide valuable insights into the mechanisms by which MC contributes to mandible development, serving as a valuable resource for future research in this area.

Organisms exhibit remarkable evolutionary diversity, with their structures adapting to complex environments (1). The skeletal system is crucial for structural support. The mandible marks a key evolutionary milestone, differentiating jawed organisms from jawless organisms and offering survival and competitive advantages (2). As the only movable bone in the craniofacial region, the mandible plays vital roles in speaking, chewing, and even predation. Its development is also integral to the development of other cranial structures, such as teeth and the temporomandibular joint (3, 4). However, the mechanisms underlying the regional differentiation of the mandible and the specific signaling pathways involved remain unclear.

Mandible development in humans begins with the migration of cranial neural crest cells (CNCCs) into craniofacial regions, where they form Meckel's cartilage (MC) between 7 and 8 postconception weeks (PCW) (5, 6). At 10 PCW, bone formation around the MC begins, with elongation and osteogenesis in its vicinity (5, 7). Traditional theories suggest that the MC primarily acts as a support for early mandible formation and serves as a template for the formation of the mandible at a later stage (8, 9). However, the gene expression of different segments of MC and their interactions with bone-forming cells are poorly understood. Single-cell RNA sequencing (scRNA-seq) and single-cell spatial enhanced resolution omics sequencing (scStereo-seq) are powerful tools for studying the diversity of cells and their spatial organization during organ development (10, 11). Therefore, a detailed, high-resolution atlas of the MC and mandibles at various stages of development is essential for further research.

Our study utilized scRNA-seq and scStereo-seq to create a spatiotemporal atlas of developing human fetal mandibles at three time points: 7 to 8, 10, and 15 PCW. This atlas revealed the diversity of cell types involved in cartilage and bone formation, differences in heterogeneous regions, and how these cells are distributed during development. We found that the anterior MC (A-MC) primarily experiences endochondral ossification, whereas the intermediate MC (I-MC) contributes to intramembranous ossification. Our study not only provides valuable human data that are supported by mouse experiments but also elucidates the role of I-MC in shaping the functionality of the mandible and potential evolutionary adaptation.

Author contributions: Z.S., R.Z., J.-K.Z., and S.W. designed research; Z.S., R.Z., X.C., G.Y., Y.S., T.Y., S.C., B.C., X.W., D.C., D.Z., and G.X. performed research; Z.S., R.Z., X.C., G.Y., Y.S., T.Y., S.C., B.C., X.W., D.C., D.Z., G.X., and J.-K.Z. analyzed data; and Z.S., R.Z., J.-K.Z., and S.W. wrote the paper.

Reviewers: J.B.G., King's College London; X.L., Zhejiang University School of Medicine; and N.O., University of Texas Health Science Center at Houston.

The authors declare no competing interest.

[1]Z.S. and R.Z. contributed equally to this work.

[2]To whom correspondence may be addressed. Email: zhujk@sustech.edu.cn or slwang@ccmu.edu.cn.

This article contains supporting information online at https://www.pnas.org/lookup/suppl/doi:10.1073/pnas.2420466122/-/DCSupplemental.

Published March 17, 2025.

Results

Spatial and Temporal Cellular Heterogeneity of the Developing Mandible. Human mandible development begins with the formation of MC. At 7 to 8 PCW, ossification starts around the MC, with observable bone formation and elongation in its vicinity. At this stage, the MC within fetal mandible sections remained undifferentiated and lacked distinct segmentation (Fig. 1*A*). At 10 PCW, the MC distinctly differentiated into A-MC and I-MC, which were associated with anterior endochondral ossification and intermediate intramembranous ossification, respectively (Fig. 1*A*). Notably, the deciduous canine germ serves as a demarcation point separating the A-MC from the I-MC (Fig. 1*A*). The anterior segment of the mandibular bone (MB) surrounding the A-MC showed signs of endochondral ossification, as chondrocyte progenitors (ProCs) gradually transformed into hypertrophic chondrocytes and were eventually replaced by osteoblasts (OBs) or osteocytes. In contrast, the intermediate segment of the mandible mainly displayed intramembranous ossification, as the ProCs did not undergo hypertrophy, and the OBs formed bone directly around the MC (Fig. 1*A*). Three-dimensional (3D) reconstructions of serial sections confirmed that the deciduous canine germ acted as the demarcation point dividing the MC into A-MC and I-MC (Fig. 1*B*). Additionally, these reconstructions revealed that the MC developed prior to mandible development, with bone growth and ossification occurring around the MC (Fig. 1*B*). The line chart illustrating the lengths of A-MC, I-MC, A-MB, and I-MB revealed that MC elongation predominantly occurred in the intermediate segment, suggesting its potential role in mandible extension and development (Fig. 1*C*).

To fully investigate the roles of MC during mandible development, human embryonic mandibles from 7 to 15 PCW were subjected to scRNA-seq and scStereo-seq analyses (Fig. 1*D*). The selected timeframe encompassed the initial establishment of ossification centers through later stages of mandibular maturation. Analysis was performed on 57,577 single cells that met the quality control standards (*SI Appendix*, Fig. S1 *A–D*). Annotations were manually assigned to various cell types, such as osteogenic cells (expressing *RUNX2* and *OMD*), chondrogenic cells (expressing *COL2A1* and *MATN3*), stromal cells (expressing *NR5A1* and *CD34*), and others (Fig. 1 *E* and *F*). Osteoblastic and chondrogenic cells were delineated into distinct subtypes on the basis of their developmental markers and temporal appearance (Fig. 1 *E* and *F* and *SI Appendix*, Fig. S1*E*). A pattern of differentiation was observed, with progenitor cell states predominantly presented at the 7 to 8 PCW and more differentiated cells starting to emerge subsequently (*SI Appendix*, Fig. S1*F*).

To complement scRNA-seq, scStereo-seq was employed to provide high-resolution spatial mapping of gene expression (*SI Appendix*, Fig. S2 *A–C*). This technique utilizes a silicon chip layered with DNA nanoballs, each carrying a unique barcode recording spatial information (12, 13). This setup allowed for the capture of mRNA from cells, and by creating pseudospots, a detailed spatially resolved map of gene expression within the mandible was obtained (14). Marker genes identified via scRNA-seq were used to visualize cell types spatially. We visualized the dynamic changes and spatial distribution of ProOBs, one of the key components in mandible development, at 7 to 8 PCW, which was the initial phase of osteogenesis, and at 15 PCW, which corresponded to a later stage of mandibular maturation. At 15 PCW, a substantial accumulation of OBs was observed, particularly at the posterior region of the I-MC, indicating their potential roles in mandibular extension and maturation. We visualized the perichondral cells (PeriChons) located at the periphery of the chondrocytes. Additionally, we mapped other essential microenvironmental cell types, including endothelial cells, immune cells, Schwann cells, and tendon cells, which contributed to the structural and functional development of the mandible (Fig. 1*G*). In summary, the integration of scRNA-seq and scStereo-seq provided a detailed atlas of cell-type-specific transcriptional changes and spatial organization during human mandible development. This comprehensive analysis highlights the dynamic interactions between key cell populations and their spatial contexts, offering critical insights into the cellular and molecular mechanisms underlying the formation and maturation of the human fetal mandible.

Dynamics and Functional Transitions of Cell Subpopulations of MC Cells During Different Developmental Stages of the Mandible. To fully investigate the roles of MC in mediating mandibular osteogenesis, we further divided MC cells into different subpopulations. Distinct clusters of MC cells, including ProCs, intermediate transitional chondrocytes (InterCs), mature chondrocytes (MatCs), hypertrophic chondrocytes (HTCs), and proliferating chondrocytes (ProfCs), were identified (Fig. 2*A*). RNA velocity analysis revealed that ProCs differentiated into InterCs, MatCs, and HTCs (Fig. 2*B*). A dot plot was used to visualize the cell markers for each MC subgroup (15, 16). All MC cell subpopulations expressed *COL2A1*, a chondrocyte lineage marker. ProCs specifically expressed *FOXP2, THBS2,* and *MEIS2*. InterCs were marked by *SCARA3*, *ANXA1,* and *CTSK*. MatCs expressed *TNFSF12A, FBXO2,* and *MATN3*. HTCs expressed *IHH, MMP13,* and *COL10A1*. ProfCs were characterized by *TOP2A, MKI67,* and *UBE2C* (Fig. 2*C* and *SI Appendix*, Fig. S3*A*). GO analysis was used to depict the functions of the marker genes for each cell type in MC (*SI Appendix*, Fig. S3*B*), with histogram and density plots showing the dynamics of MC cell subpopulations at three developmental stages. From 7 to 8 PCW to 15 PCW, as mandible development progressed, the proportions of ProCs decreased, whereas the proportions of HTCs and MatCs increased primarily after 10 PCW (Fig. 2 *D* and *E*).

The temporal distributions of the markers for these populations were also analyzed. The results revealed that at 7 to 8 PCW, ProCs and ProfCs were primarily present in the MC. After 10 PCW, few ProCs and ProfCs were present in the A-MC, whereas the majority of ProCs and ProfCs were present in the I-MC. HTCs appeared in the MC after 10 PCW and were found mainly in the A-MC (Fig. 2*F*). InterCs and MatCs were distributed both in the A-MC and I-MC (Fig. 2*F*). Based on spatial distribution, we further reclustered MC subpopulations into three groups: those present primarily in A-MC, those distributed mainly in I-MC, and those distributed throughout the entire MC (Fig. 2*G*). Further analysis of the scRNA-seq data revealed distinct markers for A-MC and I-MC cells (*SI Appendix*, Fig. S3*C*). Dot plot visualization revealed that *COL10A1* and *IBSP* were markers for A-MC cells, whereas *THBS2* and *SFRP2* were markers for I-MC cells (*SI Appendix*, Fig. S3*D*). GO enrichment analysis of these marker genes highlighted functional differences between A-MC and I-MC cells. A-MC functions were associated with the regulation of the Wnt signaling pathway and cellular stress responses (Fig. 2*H*). In contrast, I-MC cell functions were linked to connective tissue development, growth, and skeletal system development (Fig. 2*I*). In summary, through scRNA-seq and scStereo-seq profiling, we uncovered the functional roles, spatial distribution, and regulatory frameworks of MC cells during mandible development.

Potential Involvement of Early MC in Osteogenic Progenitor Cell Fate Determination. To investigate potential interactions among cells, CellPhoneDB and CellChat were used to identify ligand–receptor pairs within the major clusters. Multidirectional signaling

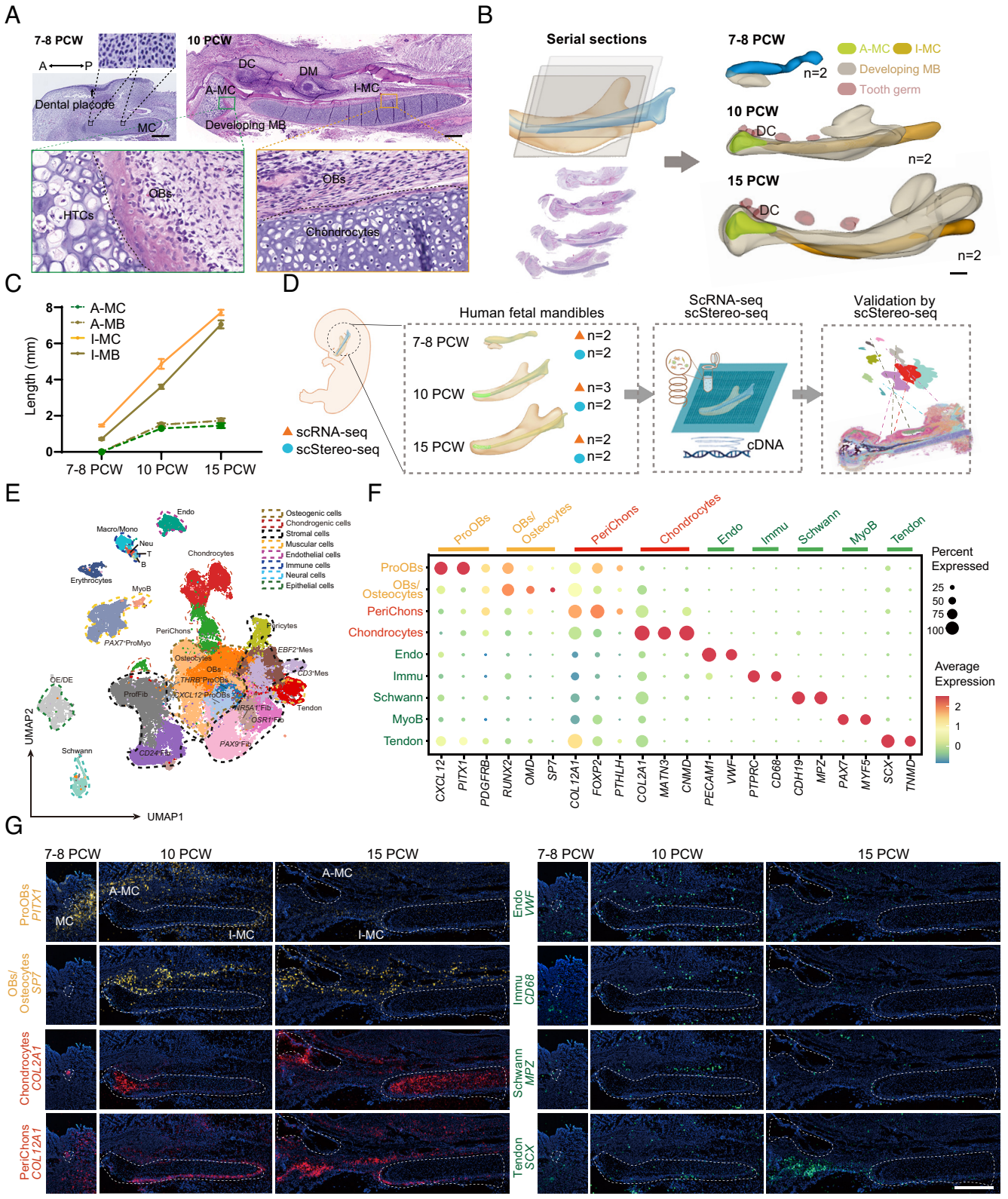

Fig. 1. Spatial and temporal cellular heterogeneity of the developing mandible. (*A*) HE staining of embryonic mandibles at the initial stage (7 to 8 PCW) and mineralization stage (10 PCW). (*B*) 3D reconstruction of serial sections showing distinct segments and spatial relationships between the MC, the tooth germ, and the developing mandibular bone at 7 to 8 PCW, 10 PCW, and 15 PCW. (*C*) Line chart illustrating the lengths of A-MC, I-MC, A-MB, and I-MB at 7 to 8 PCW, 10 PCW, and 15 PCW (n = 2). (*D*) Overview of the experimental design. (*E*) Uniform manifold approximation and projection (UMAP) plot displaying subdivided cell subpopulations. (*F*) Dot plot showing specific marker genes in the nine major cell types. The dot color represents the expression level of the marker genes in each cell. High expression levels are shown in warm hues, and low expression levels are shown in cool hues. (*G*) Visualization of marker gene expression corresponding to major cell types in developing mandibles mapped via scStereo-seq data. PCW, postconception week; MC, Meckel's cartilage; A, anterior; I, intermediate; DC, deciduous canine; DM, deciduous molar; MB, mandibular bone; OBs, osteoblasts; HTCs, hypertrophic chondrocytes; ProOBs, osteoblast progenitors; PeriChons, perichondral cells; Mes, mesenchymal cells; Fib, fibroblasts; Endo, endothelial cells; Immu, immune cells; Macro, macrophages; Neu, neutrophils; Schwann, Schwann cells; OE, oral epithelium; DE, dental epithelium; MyoB, myoblasts. (Scale bars, 200 μm in *A*; 1,000 μm in *G*.)

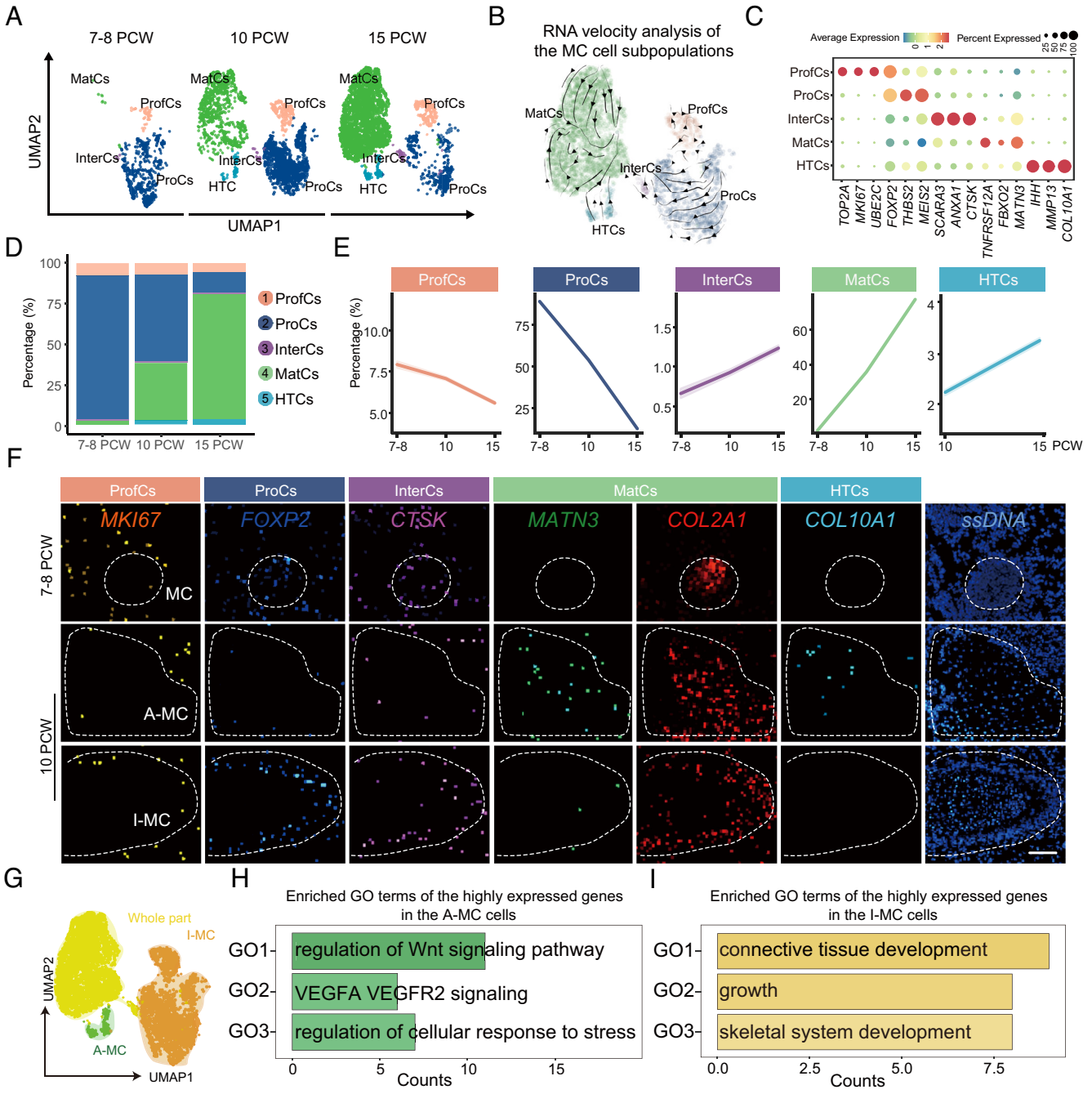

Fig. 2. Dynamics and functional transitions of cell subpopulations of MC cells during different developmental stages of the mandible. (*A*) UMAP plot displaying five distinct MC cell subpopulations across developmental stages. (*B*) RNA velocity analysis illustrating the developmental trajectories of MC cell subpopulations. (*C*) Dot plot showing specific marker genes for the five major cell subtypes. The color of the dots indicates the expression level, with warm hues representing high expression and cool hues indicating low expression. (*D*) Histogram showing the proportions of MC cell subpopulations at different developmental time points. (*E*) Line chart showing the dynamics of MC cell subpopulations at three developmental stages. (*F*) Visualization of marker gene expression in MC subpopulations during mandible development via scStereo-seq data. (*G*) Reclustering of MC cell subpopulations based on their spatial distribution. (*H* and *I*) Enriched GO terms associated with the genes most highly expressed in the A-MC and I-MC cell subpopulations. A, anterior; I, intermediate. ProfCs, proliferating chondrocytes; ProCs, chondrocyte progenitors; InterCs, intermediate transitional chondrocytes; MatCs, mature chondrocytes; HTCs, hypertrophic chondrocytes. (Scale bars, 100 μm in *F*.)

interactions among the cell clusters were visualized in circular plots (Fig. 3*A*). Notably, the chondrocytes strongly interacted with other cell clusters, particularly OBs (Fig. 3*A* and *SI Appendix*, Fig. S4 *A*–*C*). OBs are key cells involved in the intramembrane ossification center in developing mandibles. Therefore, we selected OBs and studied their interactions with chondrocytes. At 7 to 8 PCW, ProOBs were found to be close to the MC, marking the initiation of ossification centers. To further investigate these interactions, ProOBs were subclustered into two populations: *CXCL12*$^{+}$ProOBs and *THRB*$^{+}$ProOBs (Fig. 3 *B* and *C* and *SI Appendix*, Fig. S5 *A* and *B*). MC progenitors were subclustered into two populations, *CNMD*$^{+}$ProCs and *ASPN*$^{+}$ProCs, with distinct spatial distributions (Fig. 3 *B* and *C*). GO analysis of genes highly expressed in these two cartilage cell clusters revealed that *CNMD*$^{+}$ProCs were associated primarily with bone mineralization (*SI Appendix*, Fig. S5*C*), whereas *ASPN*$^{+}$ProCs were involved primarily in skeletal system development and endochondral ossification (*SI Appendix*, Fig. S5*D*). These findings demonstrated that MC progenitors play distinct functional roles during the early stages of mandible development.

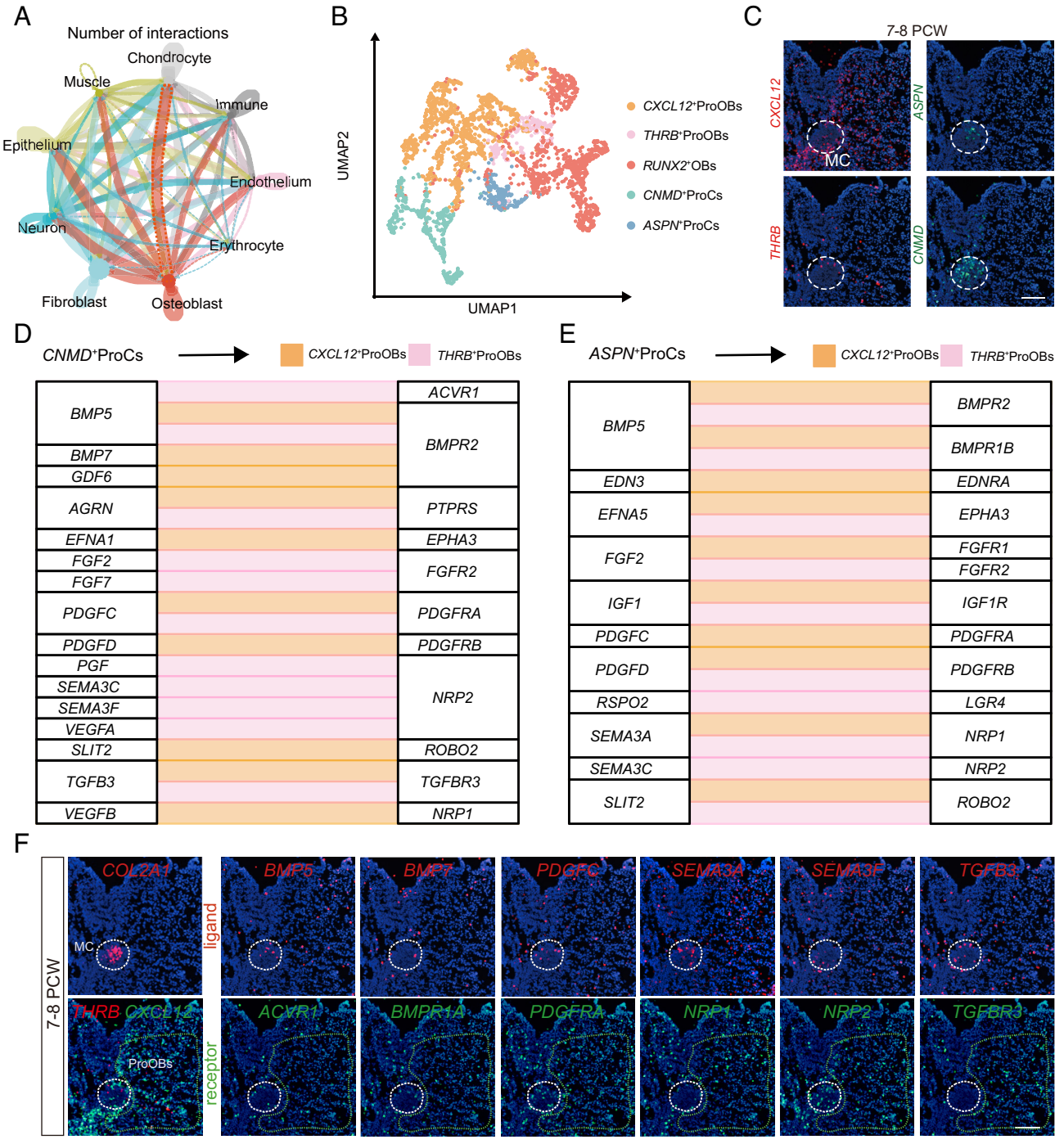

Fig. 3. Potential involvement of early MC in osteogenic progenitor cell fate determination. (*A*) Circle plot showing interactions between chondrocytes and various cell types in developing mandibles. (*B*) UMAP plot showing two subgroups of ProOBs, one group of OBs, and two subgroups of ProCs in 7 to 8 PCW mandibles. (*C*) Visualization of marker gene expression in two ProC clusters and two ProOB clusters via scStereo-seq data. (*D* and *E*) River plots showing the chosen ligand–receptor pairs in ProCs and ProOBs. (*F*) Visualization of primary ligands expressed by MC cells and corresponding receptors expressed by surrounding ProOBs via scStereo-seq data. ProCs, chondrocyte progenitors; ProOBs, osteoblast progenitors; OBs, osteoblasts. (Scale bars, 200 μm in *C* and *F*.)

Subsequent analysis via CellPhoneDB revealed strong communication signals between the two clusters of MC progenitors and ProOBs (Fig. 3*D*). A stream graph revealed that *CNMD*$^+$ProCs highly expressed *BMP5*, *TGFB3*, *BMP7*, *FGF7*, *FGF2*, *SEMA3C,* and *SEMA3CF* (Fig. 3*D*). These cytokines were previously reported to influence the aggregation and differentiation of bone cells. *ASPN*$^+$ProCs secreted cytokines, including *BMP5*, *PDGFC*, *EDN3*, *EFNA5*, *FGF2,* and *IGF1*, which may be involved in the regulation of early bone progenitor cell fate (Fig. 3*E*). Upon further visualization of the scStereo-seq results, highly and specifically expressed ligands, including *BMP5*, *BMP7*, *PDGFC*, *SEMA3A*, *SEMA3F,* and *TGFB3*, were identified in MC cells (Fig. 3*F*). The corresponding receptors expressed by ProOBs indicated that ProOBs potentially respond to these MC-derived ligands by upregulating downstream signaling pathways, thereby promoting their differentiation and migration (Fig. 3*F*). These findings suggest that early-stage MC cells may initiate the differentiation and migration of surrounding ProOBs through the production of specific ligands.

The Role of MC in the Mineralization Stage of Mandible Development. The dual-osteogenic pattern of the mandible, consisting of anterior endochondral ossification and intermediate intramembranous ossification, is believed to be responsible for normal mandible formation (17). To gain insight into the distinct roles of A-MC and I-MC cells during the mineralization stage of mandible development from 10 PCW to 15 PCW, osteogenic cells at this stage were analyzed and categorized into subgroups: ProOBs, OBs, osteocytes, and chondrocytes (Fig. 4*A*). The dot plot revealed the following cell-specific markers for each group: *CNMD* and *COL2A1* for chondrocytes; *PDGFRB*, *CXCL12,* and *PITX1* for ProOBs; *RUNX2*, *BMP5,* and *MSX1* for OBs; and *DKK1*, *DMP1,* and *CDH2* for osteocytes (15, 16) (Fig. 4*B*).

To visualize these marker genes, scStereo-seq data were employed. Spatial data analysis revealed that ProOBs were located mainly around the cartilage and beneath the oral epithelium, whereas OBs and osteocytes were located primarily on the surface of bone tissues (Fig. 4 *C* and *D*). Spatial cell velocity can provide

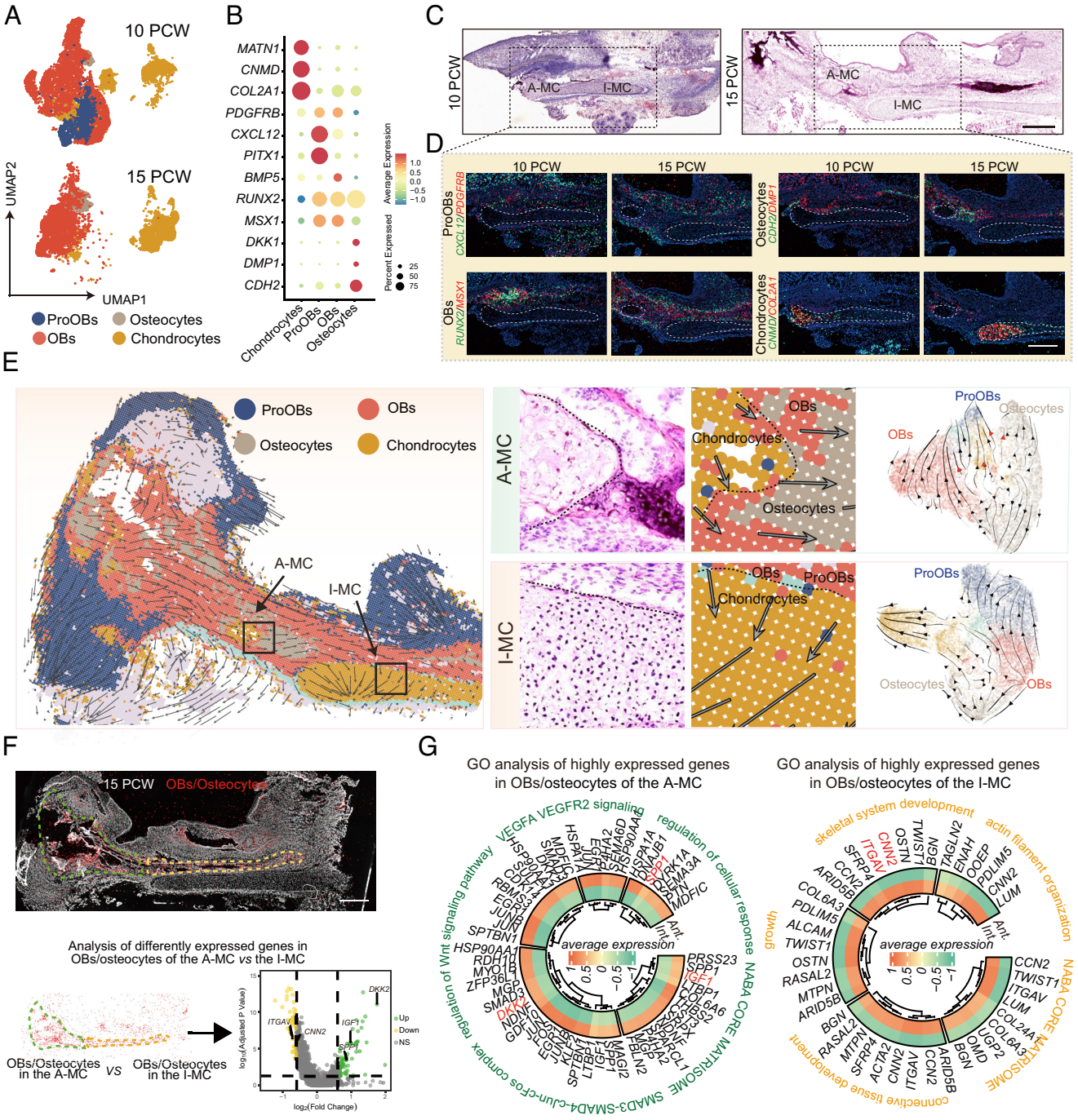

Fig. 4. The role of MC in the mineralization stage of mandible development. (*A*) UMAP plot showing ProOBs, OBs, osteocytes, and chondrocytes in developing mandibles at 10 PCW and 15 PCW. (*B*) Dot plot showing specific marker genes for the four major cell subtypes in developing mandibles at 10 PCW and 15 PCW. The color of the dots indicates the expression level, with warm hues representing high expression and cool hues indicating low expression. (*C*) HE staining of sections adjacent to those used for scStereo-seq. (*D*) Visualization of marker gene expression in each cluster in developing mandibles via scStereo-seq data. (*E*) RNA velocity streamline plots showing predicted trajectories of cell lineage transitions in the anterior and intermediate regions of the developing mandible at 15 PCW. (*F*) Analysis of DEGs in OBs/osteocytes between A-MC and I-MC. DEGs, differentially expressed genes. (*G*) GO analysis of the DEGs in OBs/osteocytes between different segments of MC. ProOBs, osteoblast progenitors; OBs, osteoblasts; A-MC, anterior Meckel's cartilage; I-MC, intermediate Meckel's cartilage. (Scale bars, 1,000 μm in *D* and *F*.)

insights into potential directions of cell differentiation (13). The scStereo-seq data were segmented into A-MC and I-MC regions to conduct spatial cell velocity analysis. Notably, red arrows highlighted the potential of A-MC cells to differentiate into ProOBs, OBs, and osteocytes, whereas I-MC cells did not show differentiation into these cell types (Fig. 4*E*). These data indicated the different fates of A-MC and I-MC, as well as different effects on the surrounding OBs/osteocytes. Supportively, GO analysis revealed that OBs/osteocytes adjacent to A-MC, which were marked by *SPP1*, *DKK2,* and *IGF1*, were enriched in cellular processes such as Wnt signaling and cellular response to stress (Fig. 4 *F* and *G*). In contrast, OBs/osteocytes surrounding I-MC exhibited a high expression of genes associated with skeletal system development and growth signaling, including *ITGAV* and *CNN2* (Fig. 4*G*). To validate these findings, we collected OBs/osteocytes from regions near and distant from the I-MC in 10 PCW human fetal mandibles and performed RNA sequencing. Osteogenesis-related genes such as *IBSP*, *SPP1*, *OSTN*, *TGFB1*, *SP7,* and *BMP4* were enriched in OBs/osteocytes proximal to I-MC, indicating that I-MC may play a critical role in promoting the osteogenic differentiation of surrounding OBs (*SI Appendix*, Fig. S6 *A–C*). These findings suggested that A-MC and I-MC contributed to mandibular osteogenesis through distinct mechanisms.

A-MC Cells Directly Convert into Osteolineage Cells. The above results implied that the mandible may contribute to osteogenesis through two different ways, anterior endochondral ossification and intermediate intramembranous osteogenesis. However, the osteogenic model of the mandible from previous studies was based on histological observations, not in vivo lineage tracing.

To test the lineage of A-MC cells, we utilized a previously reported *Col10a1-Cre;ROSA26*^{mTmG} transgenic mouse model (15), where *Cre* expression was regulated by the type X collagen gene (*Col10a1*), a specific marker for HTCs, to track the in vivo fate of A-MC. Given that MC cells contributed to osteogenesis from embryonic day 15 (E15) to postnatal day 4 (P4) (5), we examined the progeny of HTCs in the mandible at P5 (Fig. 5*A*). We found that in A-MC, GFP labeled a portion of Pdgfrb^{+} ProOBs and Ncad^{+} OBs/osteocytes, indicating that HTCs in A-MC can transdifferentiate into ProOBs and OBs. In contrast, no GFP signals were detected in the intermediate mandible, which is consistent with the fact that I-MC cells do not differentiate into HTCs (Fig. 5 *B* and *B*′).

I-MC in Mediating Mandibular Osteogenesis. We reasoned that I-MC may regulate the surrounding OBs/osteocytes through cell–cell communication. To better understand the cell–cell interactions between I-MC cells and the surrounding OBs/osteocytes, we used CellPhoneDB analysis of the scRNA-seq data and identified differentially expressed ligand–receptor pairs that may mediate communication between I-MC cells with their surrounding OBs and osteocytes. Then, these ligand–receptor interactions were validated and visualized via scStereo-seq (Fig. 6*A*). For example, three ligands, *BMP5*, *FGF7*, and *CNTN1*, which were involved in osteoblast migration and differentiation, were secreted by immature chondrocytes (Fig. 6*A*). Spatial visualization corroborated the enrichment of *BMP5*, *FGF7,* and *CNTN1* in I-MC (Fig. 6*B*). Furthermore, we identified specific transcription factors in I-MC cells. Notably, *SOX9*, a critical regulator of chondrocyte proliferation (18), was enriched in I-MC cells (Fig. 6*C*). Spatial visualization analyses, including UMAP, confirmed a specific expression of *SOX9* in MC cells at 7 to 8 PCW (Fig. 6*D*). To explore the role of *Sox9* in MC cells, we used a previously reported mouse line *Wnt1-Cre;Sox9*$^{fl/fl}$, which showed a lack of endochondral skeletal elements from CNCCs (19). Indeed, a complete absence of MC cells and mandibular shortening was observed in *Wnt1-Cre;Sox9*$^{fl/fl}$ mice (Fig. 6*E*). Immunofluorescence (IF) staining demonstrated a significantly reduced expression of several osteogenesis markers, such as Runx2 and Ibsp, in the mandibles of *Sox9* deficient embryos compared with that in the mandible of their wild-type littermates (Fig. 6 *F–H*). Additionally, IF staining showed a downregulation of osteogenesis-related ligands, including Fgf7 and Bmp5, in the intermediate mandible of *Sox9* deficient mice compared with that in the mandibles of wild-type controls (Fig. 6*I*). Taken together, these results suggest that I-MC cells may promote ossification through the secretion of some growth factors.

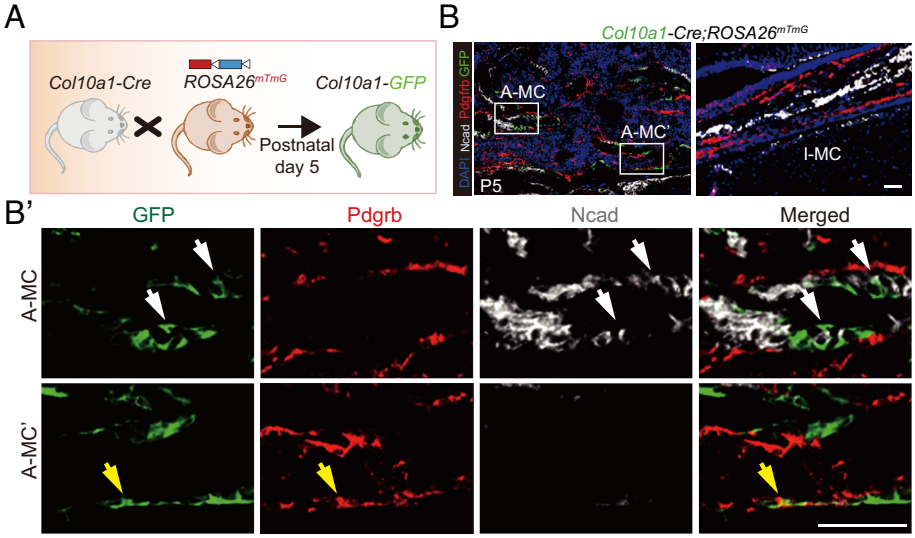

Fig. 5. A-MC cells directly convert into osteolineage cells. (*A*) Schematic representation of *Col10a1-Cre;ROSA26*^{mTmG} mice, where HTC cells and their progeny are labeled by *Col10a1-Cre*-triggered *ROSA26*^{mTmG}. (*B*) Transgenic mice traced with HTC showing that A-MC and I-MC mediate mandibular osteogenesis via distinct mechanisms. Multiplex immunostaining for Ncad and Pdgfrb identifies the locations of OBs, osteocytes, and ProOBs (n = 3). (*B*′) High-magnification images of the anterior mandible, illustrating the transdifferentiation of A-MC into ProOBs and OBs/osteocytes. OBs, osteoblasts; ProOBs, osteoblast progenitors; A-MC, anterior Meckel's cartilage; I-MC, intermediate Meckel's cartilage. (Scale bars, 100 μm in *B* and *B*′.)

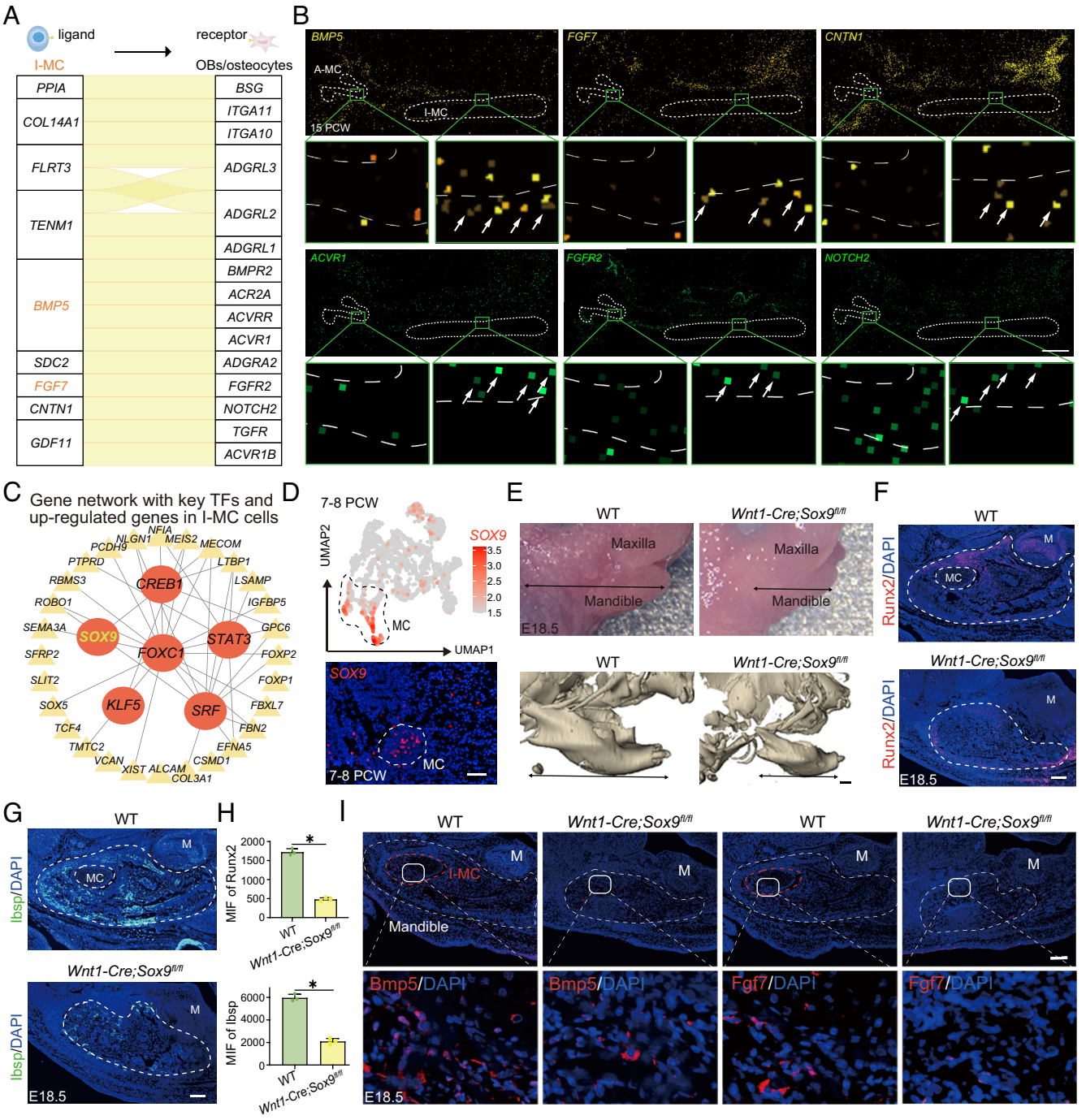

Fig. 6. I-MC in mediating mandibular osteogenesis. (*A*) River plot showing the highly expressed ligand–receptor pairs between I-MC and OBs/osteocytes. (*B*) Visualization of the highly and specifically expressed ligands in MC cells and corresponding receptors expressed in surrounding OBs/osteocytes across different segments of the developing mandible via scStereo-seq data. Arrows indicate regions within the MC with high expression in the ligands, or regions surrounding the MC with high expression in the corresponding receptors. (*C*) Gene regulatory network showing key transcription factors and marker genes of I-MC cells. (*D*) UMAP displaying the expression of *SOX9* in MC cells at 7 to 8 PCW, and further visualization of the expression of *SOX9* in MC cells at 7 to 8 PCW via scStereo-seq data. (*E*) Photographs of the WT and mutant embryos. And micro-CT imaging of the WT and mutant embryos. (*F* and *G*) Representative images of IF staining showing the expression of osteogenic markers in each group of mice. (*H*) Statistical analysis of osteogenic marker expression in each group of mice (n = 3). (*I*) IF staining showing the expression of Bmp5 and Fgf7 and in the mandibles of the WT and mutant embryos (n = 3). A-MC, anterior Meckel's cartilage; I-MC, intermediate Meckel's cartilage; OBs, osteoblasts; WT, wide-type. (Scale bars, 1,000 μm in *B*; 200 μm in *D*; 100 μm in *F*, *G*, and *I*.)

Discussion

The mandible has an intricate anatomical structure that serves crucial functions, such as chewing, swallowing, and vocalization. The complex osteogenic patterning of the mandible presents challenges in understanding the regulatory mechanisms of its development (20, 21). Because natural embryonic references are necessary for human osteogenic models but are not available, we produced a comprehensive scStereo-seq dataset with high resolution in the human fetal mandible ranging from 7 to 15 PCW. This dataset encompasses key developmental stages, from initiation to ossification, offering an opportunity to elucidate the cellular and molecular events underpinning mandible development and to explore potential pathways for therapeutic approaches in craniofacial repair and reconstruction.

Our study revealed the spatial distribution and gene expression profiles of cells throughout human fetal mandible development, including the early establishment of ossification centers and later mineralization. The MC is an essential structure in the initiation of the fetal mandible. Abnormalities in MC can lead to human disorders, such as micrognathia and mandibular hypoplasia (22). Using scRNA-seq and scStereo-seq, we identified two populations of MC progenitors in the initial stage of the fetal mandible, *CNMD*$^+$ProCs and *ASPN*$^+$ProCs, which exhibited unique spatial distributions and functions. We further identified two populations of ProOBs around ProCs, including *CXCL12*$^+$ProOBs and *THRB*$^+$ProOBs. These ProOBs played integral roles in intramembranous ossification. Furthermore, our analyses revealed critical cell types involved in mandibular mineralization, including OBs, osteocytes, PeriChons, and chondrocytes, as well as supporting microenvironmental cells such as endothelial cells, Schwann cells, and immune cells. This valuable cellular resource is essential for studying the heterogeneity and transitions of MC cells during early ossification center formation and subsequent mineralization.

Our findings elucidated how MC progenitors contributed to the establishment of early mandibular ossification centers. Previous studies lacked detailed embryonic data to address the intercellular communication mechanisms that support mandible development. By integrating scRNA-seq and scStereo-seq, we revealed extensive interactions between MC progenitors and ProOBs that potentially orchestrated the aggregation, migration, and differentiation of ProOBs at ossification centers. Specifically, *CNMD*$^+$ProCs and *ASPN*$^+$ProCs expressed ligands such as *BMP5*, *BMP7*, *SEMA3A,* and *PDGFC*, which have been reported to be involved in ProOB migration and osteogenic differentiation (23–25). The corresponding receptors expressed on ProOBs further validated the role of these signaling pathways in ossification center formation. These results indicated that the early establishment of the mandibular ossification centers was closely related to interactions between MC progenitors and ProOBs.

Our study elucidated the role of MC in anterior mandible development during the mineralization stage Previous histological studies, predominantly in murine models, described endochondral ossification in the anterior mandible (21). However, the regulatory mechanisms involved in this process remain unclear. Furthermore, there is a lack of genetic evidence regarding whether A-MC can transform into a part of the mandible (5, 6). By integrating spatial transcriptomic data with lineage tracing data, we showed that A-MC cells could differentiate into osteoblasts and osteocytes, thereby contributing to anterior mandible formation.

Our research also revealed the importance of the MC in the formation of the intermediate mandible. During the mineralization stage, we observed OBs and ProOBs closely located with I-MC. Extensive intercellular interactions between these cells and MC progenitors were identified, suggesting that I-MC might guide ProOB migration along the cartilage framework and support their differentiation into OBs and osteocytes. Specifically, I-MC cells expressed key signaling molecules such as *BMP5* (26) and *FGF7* (27), which likely played a role in recruiting ProOBs and promoting their osteogenic differentiation. *Sox9* knockout in CNCCs led to MC deficiency, with the decreased expression of both Bmp5 and Fgf7 in MC and osteogenic markers such as Runx2 and Ibsp in the intermediate mandible. These findings highlighted that I-MC promotes bone formation primarily through the secretion of osteogenic molecules. Although signaling plays an important role for I-MC, the mechanical effects of its presence and growth cannot be ignored (5), necessitating further exploration in future research.

During embryonic development, MC is responsible for the formation of the lower jaw structure in all jawed vertebrates. The MC plays a crucial and conserved role in the development and evolution of vertebrate jaws (6). Defects in MC can lead to anomalies in the size and pattern of the jaw in mouse mutants (5). In this study, we presented a detailed map of the development of the human mandible, outlining the various roles of MC in different developmental processes. Our research provides insights into the cellular and molecular mechanisms that drive mandible development, particularly the specific contributions of different MC segments to the formation of bone patterns. These data serve as a fundamental resource for understanding mandible and even tooth development, providing a foundation for advancements in craniofacial regenerative medicine.

Materials and Methods

Ethics Approval and Consent. Ethics approval for this study was granted by the Institutional Review Boards of Beijing Friendship Hospital, Capital Medical University (2021-P2-198-02), and Beijing Children's Hospital, Capital Medical University (2023-KY-082-01). All procedures involving human mandibles were conducted in accordance with the principles outlined in the Declaration of Helsinki. Informed consent was obtained from all donors or their legal representatives prior to the acquisition of mandibles.

Source of Mandibles. Fifteen human fetal mandibles were obtained with written informed consent from the donor couples at Beijing Friendship Hospital and Beijing Children's Hospital. The consents confirmed that the couples voluntarily donated embryos for research on the mechanisms of human mandible development, with no financial compensation. Eligible participants were of childbearing age and had no history of hypertension, diabetes, systemic diseases, or infectious diseases. The pregnancies were natural conceptions, and the participants were not exposed to chemical drugs or radiation during preconception or early pregnancy. Additionally, they had not taken teratogenic medications (e.g., quinolones, tetracyclines) or contracted viral infections (e.g., rubella, Toxoplasma, *Treponema*) during pregnancy. Furthermore, there were no familial genetic disorders, including inherited malformations, chromosomal abnormalities, or gene mutations in embryonic cells. Mandibles from anatomical donation programs were acquired through standardized anatomical dissection procedures conducted by trained anatomists.

Ethical Considerations. Respect for donors: Mandibles were handled with respect and dignity, and efforts were made to honor the wishes of donors and their families. Privacy and confidentiality: Donor information was kept confidential, and mandibles were used only for authorized research purposes. Compliance with regulations: Mandible acquisition and use complied with all applicable regulations governing the handling and use of human tissue.

Sample Collection and Preparation. Single-cell suspensions were prepared from the mandibles of embryos at 7 to 8 PCW, 10 PCW, and 15 PCW. Human fetal mandibles were dissociated into single-cell suspensions through a combination of enzymes, including trypsin and type I collagenase, and mechanical dissociation methods. Cell viability was assessed via trypan blue exclusion or other appropriate methods to ensure high-quality single-cell suspensions.

Library Preparation and scRNA-seq. Library preparation and scRNA-seq were performed according to 10× Genomics' technical standards. Specifically, single cells were individually barcoded using unique molecular identifiers (UMIs) or cell-specific barcodes to distinguish between cells during downstream analysis. The mRNA from each cell was reverse transcribed into complementary DNA (cDNA) using oligo(dT) primers or random primers. cDNA was amplified using PCR to generate sufficient material for sequencing. scRNA-seq libraries were sequenced to generate high-throughput sequencing data. The raw sequencing reads were aligned to the reference genome or transcriptome using alignment algorithms. Low-quality cells and reads with low mapping quality or high duplication rates were filtered out on the basis of predefined quality metrics.

Tissue Sectioning. Fresh-frozen tissue samples were sectioned into thin slices (10 μm thick) using a cryostat or microtome. The tissue sections were mounted onto glass slides or specialized spatial capture devices compatible with the chosen scStereo-seq technology.

Library Preparation and scStereo-seq. Mandible sections were affixed onto STOmics® chips. After fixation and permeabilization, the spatially labeled probe present on the chip surface facilitated the capture of released mRNA molecules for subsequent library construction and sequencing (28, 29). The STAR algorithm was employed to align the clean Read1 and Read2 sequences with the reference genome. With Bam2Gem software, comprehensive gene information from all the tissue section locations captured by the STOmics® chip probes was obtained. The expression levels of genes were subsequently calculated on the basis of corrected MIDs, which are distinct barcode sequences utilized in high-throughput sequencing to differentiate various libraries within a combined sequencing pool.

Data Preprocessing and Quality Control. Data analysis was performed via R software (v4.1.0). Seurat (v4.0.0) was used to read the data and filter out low-quality cells. Data normalization methods were applied to correct for sequencing depth and cell-specific biases. Batch effects arising from differences in experimental conditions or sequencing runs were corrected via Harmony (v.1.2.0) to harmonize the datasets.

Data Analysis. For the scStereo-seq data, a binned (bin 50, 50 × 50 DNB bins, 25 μm diameter) expression matrix was created as previously described. Principal component analysis (PCA) and UMAP were used for dimensionality reduction to visualize cell–cell relationships. The cells were clustered on the basis of differential expression analysis or known marker gene sets from the literature or databases. The defined cell types were further validated based on their spatial distribution characteristics. For the scRNA-seq data, the cell clusters were annotated to known cell types via marker gene expression profiles, cell-type-specific gene signatures, or known marker gene sets from the literature. Genes that were differentially expressed between clusters or experimental conditions were identified via statistical tests via the Seurat package.

Gene Visualization via scStereo-seq. The scStereo-seq platform was utilized to visualize the spatial expression of marker genes associated with major cell types, as well as selected ligands in MC cells. The scStereo-seq platform is a high-resolution spatial transcriptomics technology that enables the profiling of gene expression at the single-cell level while preserving tissue architecture. The gene expression heatmap of the stereo-seq data was created using the visualization tool StereoMap (V4.1), which can be accessed at https://www.stomics.tech/.

Cell–Cell Communication Analysis. CellPhoneDB and CellChat were used to analyze cell–cell communication networks from the scRNA-seq data. CellPhoneDB is a publicly available database and computational tool designed to identify potential ligand–receptor pairs based on the expression levels of ligand and receptor genes across different cell populations. Processed scRNA-seq data and cell type annotations were input into CellPhoneDB (v.5.0.0) to identify interactions between cells. Hypergeometric and permutation tests were performed to assess the significance of these ligand–receptor interactions. Interaction matrices and network diagrams were visualized via the use of libraries such as matplotlib (v.3.7.2).

In addition to CellPhoneDB, CellChat (v.1.6.0) was employed for a more comprehensive analysis of intercellular communication. CellChat uses known signaling pathways to infer the communication between cells by modeling the transmission of signaling messages through ligands, receptors, and downstream signaling networks. The processed transcriptomic data, including cell type annotations, were analyzed with CellChat to construct a communication network. CellChat calculates the communication probability, identifies the key signaling pathways, and visualizes the intercellular communication landscape via network diagrams. Statistical tests, including permutation and bootstrap methods, were used to assess the significance of the interactions, and the results were visualized as communication networks to reveal the most active signaling pathways between cell types.

3D Construction. Sixty-two 7 to 8 PCW, seventy-seven 10 PCW, and one hundred and fifty-eight 15 PCW serial mandible sections were acquired for 3D construction. Image segmentation was performed to identify and delineate relevant structures or objects of interest within the images. Once segmented, the boundaries of the objects were used to reconstruct their 3D surfaces. Various algorithms, such as marching cubes or surface fitting techniques, have been employed to generate a continuous surface mesh that represents the geometry of objects. Mesh refinement techniques, including smoothing, decimation, and surface fitting, were applied to improve the quality of the mesh and ensure geometric accuracy. The reconstructed 3D models were visualized via 3D Mimics software, and the material properties were adjusted to enhance the visual appearance of the model and facilitate interpretation.

Mice. Standard rodent chow and water were provided ad libitum throughout the study. Genomic DNA was extracted from mouse tail biopsies, and PCR was performed to confirm the presence of the *Wnt1-Cre;Sox9*$^{fl/fl}$ and *Col10a1-Cre;ROSA26*^{mTmG} alleles in each mouse. *Wnt1-Cre* mice were purchased from the Jackson Laboratory (003829), while *Col10a1*^{int2}*-Cre* and *Sox9*$^{fl/fl}$ mice were previously described (30). Efforts were made to minimize animal suffering and reduce the number of animals used in accordance with the principles of the 3Rs (replacement, reduction, and refinement).

Statistical Analyses. ScRNA-seq and scStereo-seq data were analyzed via R software and are presented as the means ± SEMs. Statistical comparisons between groups were conducted via the Wilcoxon test, with the significance threshold set at $P < 0.05$. Other data types were analyzed via GraphPad Prism 8.0, and the results are presented as the means ± SEMs. Statistical comparisons were performed via Student's *t* test at a significance threshold of $P < 0.05$.

Data, Materials, and Software Availability. The raw sequence data reported in this paper have been deposited in the database of the CNGB Sequence Archive (CNSA). The raw data of scRNA-seq and scStereo-seq are publicly accessible on project CNP0006081 (31). This paper does not report the original code. Any additional information required to reanalyze the data reported in this paper is available from the corresponding author upon request. All other data are included in the manuscript and/or *SI Appendix*.

ACKNOWLEDGMENTS. This work was supported by the National Natural Science Foundation of China (82030031); the Chinese Research Unit of Tooth Development and Regeneration, Academy of Medical Sciences (2019-12M-5-031); the National Key Research and Development Program (2022YFA1104401); a Beijing Municipal Government grant (Beijing Laboratory of Oral Health, PXM2021-014226-000041); the Beijing Municipal Government (Beijing Scholar Program, PXM2021-014226-000020); the National Natural Science Foundation of China (92149301, L2224038, 82201011, and 82270945); and the Innovation Research Team Project of Beijing Stomatological Hospital, Capital Medical University (CXTD202201). We would like to thank Prof. Yan Teng for her invaluable assistance in revising the manuscript. We would like to thank Yunjia Huang and Jiayu Yang for their invaluable assistance in bioinformatics analysis. We would like to thank Prof. Guan Yang for providing *Sox9*$^{fl/fl}$ mice and *Col10a1-Cre;ROSA26*^{mTmG} mice. We would like to thank Prof. Ruili Yang for providing the *Wnt1-Cre* mice.

Author affiliations: [a]Beijing Laboratory of Oral Health, School of Basic Medical Sciences, Capital Medical University, Beijing 100069, China; [b]Immunology Research Center for Oral and Systemic Health, Beijing Friendship Hospital, Capital Medical University, Beijing 100050, China; [c]Department of Periodontology, Hospital of Stomatology, Sun Yat-Sen University, Guangzhou 510055, China; [d]Department of Oral Pathology, Peking University School and Hospital of Stomatology, Beijing 100081, China; [e]State Key Laboratory of Medical Proteomics, Beijing Proteome Research Center, National Center for Protein Sciences, Beijing Institute of Lifeomics, Beijing 102206, China; [f]Department of Reproductive Regulation, Beijing Obstetrics and Gynecology Hospital, Capital Medical University, Beijing 100026, China; [g]Academician Workstation for Oral-Maxillofacial Regenerative Medicine, Central South University, Changsha 410008, China; [h]Faculty of Pharmaceutical Sciences, Shenzhen University of Advanced Technology, Shenzhen 518107, China; [i]Department of Biochemistry, Homeostatic Medicine Institute, School of Medicine, Shenzhen Key Laboratory of Cell Microenvironment, Guangdong Provincial Key Laboratory of Cell Microenvironment and Disease Research, Southern University of Science and Technology, Shenzhen 518055, China; [j]Institute of Advanced Biotechnology, School of Medicine and Homeostatic Medicine Institute, Southern University of Science and Technology, Shenzhen 518055, China; and [k]Laboratory of Homeostatic Medicine, School of Medicine and Homeostatic Medicine Institute, Southern University of Science and Technology, Shenzhen 518055, China

1. Y. Shao *et al.*, Phylogenomic analyses provide insights into primate evolution. *Science* **380**, 913–924 (2023).
2. Y. A. Zhu *et al.*, The oldest complete jawed vertebrates from the early Silurian of China. *Nature* **609**, 954–958 (2022).
3. B. S. Bhullar *et al.*, Rolling of the jaw is essential for mammalian chewing and tribosphenic molar function. *Nature* **566**, 528–532 (2019).
4. M. Zhu *et al.*, A Silurian maxillate placoderm illuminates jaw evolution. *Science* **354**, 334–336 (2016).
5. E. Svandova, N. Anthwal, A. S. Tucker, E. Matalova, Diverse fate of an enigmatic structure: 200 years of Meckel's cartilage. *Front. Cell Dev. Biol.* **8**, 821 (2020).
6. Y. Yuan, Y. Chai, Regulatory mechanisms of jaw bone and tooth development. *Curr. Top Dev. Biol.* **133**, 91–118 (2019).
7. M. Wyganowska-Świątkowska, A. Przystańska, The Meckel's cartilage in human embryonic and early fetal periods. *Anat. Sci. Int.* **86**, 98–107 (2011).
8. G. C. Schoenwolf, S. C. Bleyl, P. R. Brauer, P. H. Francis-West, "Development of the pharyngeal apparatus and face" in *Larsen's Human Embryology* (Elsevier, 2008), pp. 543–582.
9. A. Nanci, "Embryology of the head, face, and oral cavity" in *Ten Cate's Oral Histology* (Elsevier, 2012), pp. 24–47.
10. S. Bandyopadhyay *et al.*, Mapping the cellular biogeography of human bone marrow niches using single-cell transcriptomics and proteomic imaging. *Cell* **187**, 3120–3140.e9 (2024).
11. Y. Li *et al.*, Spatiotemporal transcriptome atlas reveals the regional specification of the developing human brain. *Cell* **186**, 5892–5909.e2 (2023).
12. A. Chen *et al.*, Single-cell spatial transcriptome reveals cell-type organization in the macaque cortex. *Cell* **186**, 3726–3743.e24 (2023).
13. X. Wei *et al.*, Single-cell Stereo-seq reveals induced progenitor cells involved in axolotl brain regeneration. *Science* **377**, eabp9444 (2022).
14. J. Frommer, M. R. Margolies, Contribution of Meckel's cartilage to ossification of the mandible in mice. *J. Dent Res.* **50**, 1260–1267 (1971).
15. G. Yang *et al.*, Identification of the metaphyseal skeletal stem cell building trabecular bone. *Sci. Adv.* **10**, eadl2238 (2024).
16. B. Zhang *et al.*, A human embryonic limb cell atlas resolved in space and time. *Nature* **635**, 668–678 (2024), 10.1038/s41586-023-06806-x.
17. C. Parada, Y. Chai, Mandible and tongue development. *Curr. Top Dev. Biol.* **115**, 31–58 (2015).
18. K. Mizuhashi *et al.*, Resting zone of the growth plate houses a unique class of skeletal stem cells. *Nature* **563**, 254–258 (2018).
19. Y. Mori-Akiyama, H. Akiyama, D. H. Rowitch, B. de Crombrugghe, Sox9 is required for determination of the chondrogenic cell lineage in the cranial neural crest. *Proc. Natl. Acad. Sci. U.S.A.* **100**, 9360–9365 (2003).
20. M. Farahat, G. A. S. Kazi, E. S. Hara, T. Matsumoto, Effect of biomechanical environment on degeneration of Meckel's cartilage. *J. Dent. Res.* **100**, 171–178 (2021).
21. M. Biosse Duplan *et al.*, Meckel's and condylar cartilages anomalies in achondroplasia result in defective development and growth of the mandible. *Hum. Mol. Genet.* **25**, 2997–3010 (2016).
22. S. Mansour *et al.*, The phenotype of survivors of campomelic dysplasia. *J. Med. Genet.* **39**, 597–602 (2002).
23. R. Wu *et al.*, A novel human long noncoding RNA SCDAL promotes angiogenesis through SNF5-mediated GDF6 expression. *Adv. Sci. (Weinh)* **8**, e2004629 (2021).
24. Y. Han, X. You, W. Xing, Z. Zhang, W. Zou, Paracrine and endocrine actions of bone-the functions of secretory proteins from osteoblasts, osteocytes, and osteoclasts. *Bone Res.* **6**, 16 (2018).
25. M. Wu, S. Wu, W. Chen, Y. P. Li, The roles and regulatory mechanisms of TGF-β and BMP signaling in bone and cartilage development, homeostasis and disease. *Cell Res.* **34**, 101–123 (2024).
26. H. Y. Shih *et al.*, Bmp5 regulates neural crest cell survival and proliferation via two different signaling pathways. *Stem Cells* **35**, 1003–1014 (2017).
27. X. Liu *et al.*, FGF7-induced E11 facilitates cell-cell communication through connexin43. *Int. J. Biol. Sci.* **17**, 3862–3874 (2021).
28. Y. Lei *et al.*, Region-specific transcriptomic responses to obesity and diabetes in macaque hypothalamus. *Cell Metab* **36**, 438–453e6 (2024).
29. Z. Shen *et al.*, Restoring periodontal tissue homoeostasis prevents cognitive decline by reducing the number of Serpina3n(high) astrocytes in the hippocampus. *Innovation (Camb)* **5**, 100547 (2024).
30. G. Yang *et al.*, Osteogenic fate of hypertrophic chondrocytes. *Cell Res.* **24**, 1266–1269 (2014).
31. Z. Shen, R. Zhang, J.-K. Zhu, S. Wang, Single-cell sequencing and spatial transcriptomics analysis of mandibular development. CNGB Sequence Archive (CNSA) of China National GeneBank DataBase (CNGBdb). https://db.cngb.org/search/?q=CNP0006081. Deposited 12 August 2024.